


RESEARCH ARTICLE

Applying remote sensing for large-landscape problems: Inventorying and tracking habitat recovery for a broadly distributed Species At Risk

Melanie Dickie¹  | Branislav Hricko¹ | Christopher Hopkinson² | Victor Tran¹ | Monica Kohler¹ | Sydney Toni¹ | Robert Serrouya¹  | Jahan Kariyeva^{1,3}

¹Alberta Biodiversity Monitoring Institute, University of Alberta, Edmonton, Alberta, Canada

²Department of Geography & Environment, University of Lethbridge, Lethbridge, Alberta, Canada

³Canadian Wildlife Service, Pacific Region, Environment and Climate Change Canada, Delta, British Columbia, Canada

Correspondence

Melanie Dickie

Email: mvezina@ualberta.ca

Funding information

North West Species At Risk Committee

Handling Editor: Jonas Hagge

Abstract

1. Anthropogenic habitat alteration is leading to the reduction of global biodiversity. Consequently, there is an imminent need to understand the state and trend of habitat alteration across broad areas. In North America, habitat alteration has been linked to the decline of threatened woodland caribou. As such, habitat protection and restoration are critical measures to support recovery of self-sustaining caribou populations. Broad estimates of habitat change through time have set the stage for understanding the status of caribou habitat. However, the lack of updated and detailed data on post-disturbance vegetation recovery is an impediment to recovery planning and monitoring restoration effectiveness. Advances in remote sensing tools to collect high-resolution data at large spatial scales are beginning to enable ecological studies in new ways to support ecosystem-based and species-based management.
2. We used semi-automated and manual methodologies to fuse photogrammetry point clouds (PPC) from high-resolution aerial imagery with wide-area light detection and ranging (LiDAR) data to quantify vegetation structure (height, density, class) on disturbances associated with caribou declines. We also compared vegetation heights estimated from the semi-automated PPC-LiDAR fusion to heights estimated in the field, using stereoscopic interpretation, and using multi-channel TiTAN LiDAR.
3. Vegetation regrowth was occurring on many of the disturbance types, though there was local variability in the type, height and density of vegetation. Heights estimated using PPC-LiDAR fusion were highly correlated ($r \geq 0.87$ in all cases) with heights estimated using stereomodels, TiTAN multi-channel LiDAR and field measurements.
4. We demonstrated that PPC-LiDAR fusion can be operationalized over large areas to collect comprehensive and consistent vegetation data across landscape levels, providing opportunities to link fine-resolution remote sensing to landscape-scale

This is an open access article under the terms of the [Creative Commons Attribution](https://creativecommons.org/licenses/by/4.0/) License, which permits use, distribution and reproduction in any medium, provided the original work is properly cited.

© 2023 The Authors. *Ecological Solutions and Evidence* published by John Wiley & Sons Ltd on behalf of British Ecological Society.

ecological studies. Crucially, these data can be used to estimate rates of habitat recovery at resolutions that are not feasible using more commonly used satellite-based sensors, bridging the gap between resolution and extent. Such data are needed to achieve effective and efficient habitat monitoring to support caribou recovery efforts, as well as a myriad of additional forest management needs.

KEYWORDS

habitat assessment, light detection and ranging, photogrammetry, *Rangifer tarandus*, vegetation recovery

1 | INTRODUCTION

Habitat alteration, as a result of both human land-use and climate change, is disrupting ecosystem processes and leading to the decline of many species across the globe (Betts et al., 2022; Foley et al., 2005; Newbold et al., 2015). The link between habitat alteration and biodiversity declines necessitates assessments of the impacts of habitat change on ecological systems (Díaz et al., 2020; Hansen et al., 2013; Tschardt et al., 2012). Given the need for habitat assessment is largely global, monitoring and managing problems at regional landscapes is critical (Tschardt et al., 2012). Measuring and tracking habitat often comes with a trade-off between extent and resolution, and too often a disconnect exists between the information available and the information needed to appropriately understand the status and trend of habitat. The combination of remote sensing tools and ecological research is coming together in promising ways to support species- and ecosystem-based management over broad areas (Cavender-Bares et al., 2022; Queinnec et al., 2021). Large-scale habitat inventories will be necessary for future wildlife, habitat, and land-use management, understanding how global change influences ecological processes and how restoration ecology can address these changes.

Traditionally, habitat assessments have been conducted using field-based sampling to assess metrics of vegetation structure. While these fine-scale assessments are important for activities such as habitat restoration treatment monitoring (Filicetti et al., 2019; Fromm et al., 2019), they lead to inconsistent data collection across landscapes (Fromm et al., 2019; Luoma et al., 2017). At larger scales, forest inventories have traditionally been conducted using remote sensing tools such as aerial imagery and stereoscopic visualization, with recent advances such as the use of photogrammetry point clouds (PPC) supporting more detailed mapping of forest structure (Dietmaier et al., 2019; Jurado et al., 2022). Airborne and terrestrial laser scanning data, such as light detection and ranging (LiDAR), and imagery-based photogrammetry with horizontal and vertical accuracies of centimetres to meters across wide-areas provide the spatial continuity and resolution required for many applications (Hopkinson et al., 2016; Queinnec et al., 2021; Wulder et al., 2012). At larger scales still, satellite-based imagery or laser scanning data are becoming increasingly available at sufficient resolutions for some tasks (Jurado et al., 2022; Nasiri et al., 2022). With the increasing availability of high-resolution data across landscapes, and ability to combine

multiple data types (Jurado et al., 2022; Nasiri et al., 2022; Zhang & Lin, 2017), comes improved integration of remote sensing with ecological studies.

The boreal forests of Canada are relatively intact compared to other nations (Coristine et al., 2019; Watson et al., 2016); yet, the cascading influence of anthropogenic habitat alteration has been linked to the decline of threatened woodland caribou (*Rangifer tarandus caribou*, hereafter termed 'caribou'). Caribou habitat overlaps areas with high value for forestry and energy resources (Hebblewhite, 2017). As such, caribou ranges across western Canada are facing accelerating habitat loss (Nagy-Reis et al., 2021). Anthropogenic habitat alteration in particular has changed the predator-prey dynamics and ecological processes in which caribou evolved. Vegetation regrowth in polygonal disturbances (e.g. forest harvest areas) provides competing ungulates with increased forage availability (Serrouya et al., 2011). The resulting increase in the density of competing ungulates, such as white-tailed deer *Odocoileus virginianus* and moose *Alces alces*, which have higher fecundity than caribou, augments predator numbers and leads to unsustainable predation on caribou (Serrouya et al., 2021; Wittmer et al., 2005). Furthermore, energy developments in the boreal forests create linear forest clearings such as pipelines, roads and seismic lines used to delineate and access oil and gas reserves underground (termed 'linear features'). These narrow linear features are associated with increased hunting efficiency of predators such as wolves *Canis lupus* (Dickie, Serrouya, McNay, et al., 2017; McKenzie et al., 2012), increased predator use of caribou habitat (DeMars & Boutin, 2017) and increased caribou predation (McKay et al., 2021).

Effective habitat management, including protection and restoration, requires up-to-date and accurate information about habitat status and post-disturbance vegetation recovery. Within the context of recovering threatened caribou populations, recent work has set the stage by estimating the net rate of change in forest cover by quantifying habitat loss and gain across western Canada's caribou ranges (Nagy-Reis et al., 2021). While these satellite-based metrics provide consistent and replicable tracking across large areas, the lack of updated and detailed vegetation data across the vast areas of the boreal forest has been highlighted as an impediment to recovery planning, especially because many disturbance types are poorly tracked using traditional remote sensing methods (Nagy-Reis et al., 2021). Localized studies have revealed thresholds between vegetation structure and reduced travel speed by both wolves and

humans on linear features (Dickie, Serrouya, DeMars, et al., 2017; Finnegan, Pigeon, et al., 2018; Pigeon et al., 2016). Likewise, the replacement of mature trees with early-seral forage, particularly within polygonal features such as forest harvest areas, is linked to increased use and abundance of ungulates such as moose (Mumma et al., 2020), with an expected increase in wolf abundance and therefore decreased caribou persistence (Wittmer et al., 2007). Therefore, vegetation height and density by class (i.e. shrub versus coniferous or deciduous trees) are considered key metrics to track the functional recovery of caribou habitat. However, given the magnitude of anthropogenic habitat alteration within boreal caribou ranges (Nagy-Reis et al., 2021), tracking post-disturbance recovery at scale remains a daunting challenge.

Despite the growing evidence that optical and laser-scanning data can provide accurate estimations of vegetation structure (St-Onge et al., 2015; Wang et al., 2019), the use of high-resolution forest structure information has yet to be widely adopted in ecological studies. We demonstrate the use of high-resolution remote sensing across broad areas to collect up-to-date and accurate information on post-disturbance vegetation structure to support tracking habitat change for a threatened ungulate. We first fuse PPC from high-resolution aerial imagery with LiDAR data to quantify vegetation structure on polygonal and linear features associated with caribou declines. We interpret these vegetation metrics within the context of caribou habitat recovery. We then validated vegetation structure metrics derived from PPC-LiDAR fusion by comparing them to field-based measurements (i.e. the 'gold standard' for validation), manual stereoscopic visualization (i.e. a traditional technique for remotely sensed vegetation inventorying), and multi-channel TiTAN LiDAR measurements (Hopkinson et al., 2016; i.e. a state-of-the-art technique for high-resolution remotely sensed vegetation inventorying). Finally, we discuss data limitations and the next steps for the application of these methods to support local and regional vegetation assessments and habitat management.

2 | MATERIALS AND METHODS

We leveraged two data sets to measure post-disturbance vegetation recovery on polygonal and linear features linked to caribou declines. On most disturbance types, we fused a digital surface model (DSM) derived from high-resolution optical imagery PPC with a bare earth digital terrain model (DTM) derived from wide-area LiDAR in a semi-automatic process to quantify structure (height and density) of shrubs and trees. PPC provides estimates of tree-top locations, but visual obstruction of the ground creates difficulties with accurately estimating bare earth (and so, height). We therefore used previously collected wide-area LiDAR data to derive bare earth measurements. Wide-area LiDAR data with older vintages are often not collected at sufficient resolutions for estimating vegetation metrics, but do provide useful information on bare earth. The fusion of these two data sets allowed us to first estimate tree-top locations, and second subtract the difference between the two metrics (DSM-DTM),

yielding estimates of vegetation height. Using this semi-automated process, we combined the tree-top locations with estimated heights to estimate the height and density of trees post-disturbance across large areas. We supplemented the semi-automated PPC-LiDAR process using stereoscopic interpretation of vegetation structure and class on narrower features, such as seismic lines, where adjacent canopy prohibited the automated PPC-LiDAR process. We first describe the methodological details developed to estimate vegetation structure using PPC-LiDAR fusion (Developing and applying PPC-LiDAR fusion), then describe the methodology used to validate our PPC-LiDAR height measurements (Testing accuracy of vegetation height estimates).

2.1 | Developing and applying PPC-LiDAR fusion

2.1.1 | Study area

We assessed post-disturbance vegetation recovery at approximately 20 townships (~94 km² per township; total of 1883 km²) distributed across four areas in northwestern Alberta, Canada (Figure 1) in two caribou ranges. The Chinchaga (17,643.64 km²) and Caribou Mountains (20,658.73 km²) caribou ranges are located in the boreal forest of northwestern Alberta. The area is characterized by a mosaic of upland forests dominated by white spruce *Picea glauca*, trembling aspen *Populus tremuloides*, and balsam poplar *Populus balsamifera*, mixed with poorly drained lowlands. The Caribou Mountains caribou range overlaps a low plateau left unglaciated during the last ice age, leaving behind unique remnant communities of lichens, vascular plants and mosses not found in the surrounding areas.

Approximately 19% of the boreal forests of Alberta are directly impacted by human footprint (Alberta Biodiversity Monitoring Institute, 2018a). The majority of this human footprint is from the agriculture (11.5%), forestry (3.8%) and energy (1.8%) sectors. Approximately 74% of the Chinchaga range and 23% of the Caribou Mountains range is influenced by anthropogenic habitat alteration (defined as habitat alteration buffered by 500m; Environment Canada, 2012; Environment and Climate Change Canada, 2017). Additionally, fire impacts approximate 8% of the Chinchaga range and 44% of the Caribou Mountains range.

2.1.2 | Data collection

We produced a DSM using PPC data derived from optical imagery. Imagery was acquired using a Piper PA31 Navajo aircraft during the leaf-on season of 2020 (September 8, 10 and 22) across three areas in Chinchaga (C1: 380.03 km², C2: 379.93 km², C3: 383.79 km²) and two areas in Caribou Mountains that were then combined (CM: 739.43 km²). Imagery was flown at an average altitude of 3550m above terrain. The areas were selected based on overlap with caribou range, presence of energy footprint and accessibility for field measurements. We used a high-end, large-frame Leica Digital

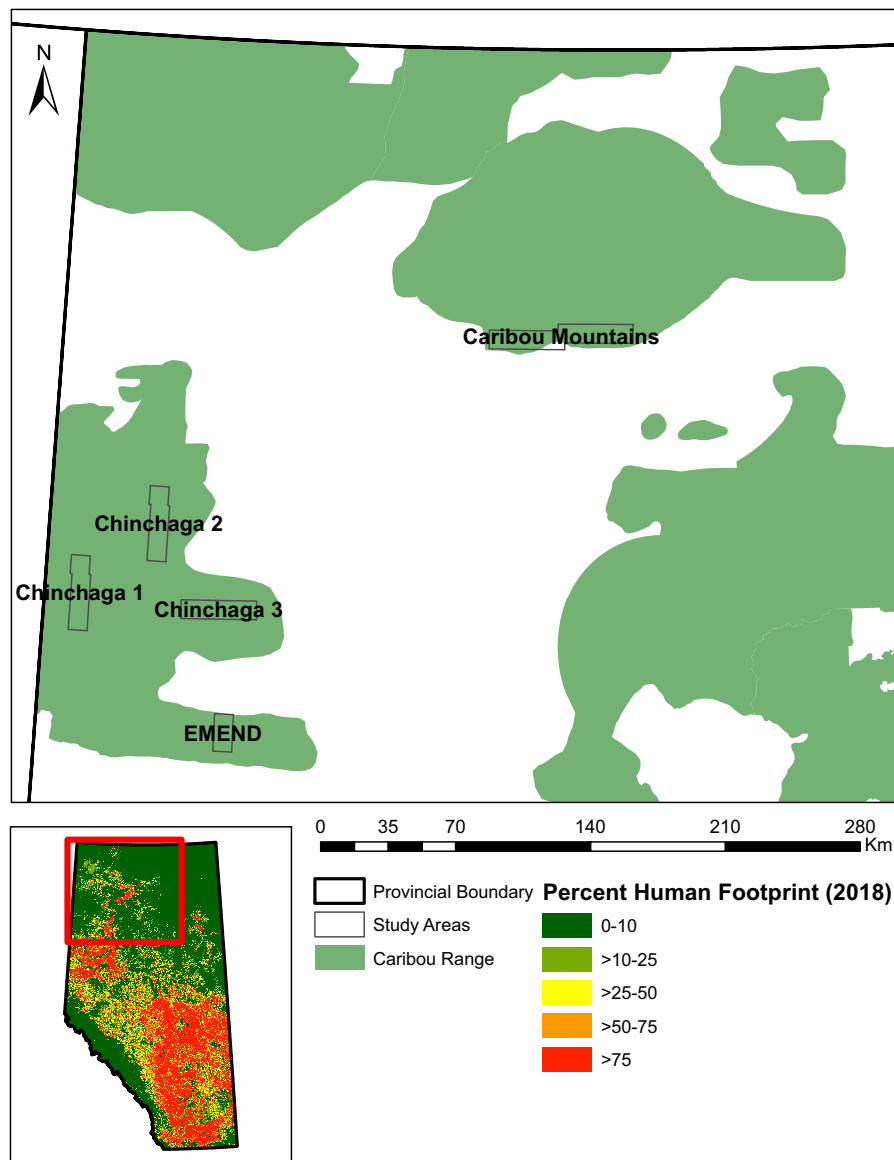


FIGURE 1 Study area locations, including the independent testing location (Ecosystem Management Emulating Natural Disturbance [EMEND] project), in relation to boreal caribou range in northwestern Alberta. Inset map shows the percent human footprint across Alberta (Alberta Biodiversity Monitoring Institute, 2018b) for reference.

Media Camera (DMC) III Airborne Digital Camera, manufactured by Hexagon, Leica Geosystem. DMC III uses Complementary Metal Oxide Semiconductor sensor technology and has five lens configurations, each for a separate spectral band (Panchromatic, Red, Green, Blue and Near-Infrared). The Near-Infrared band reflects chlorophyll more than other bands, and so is key to classifying vegetation. We captured images with below 15-cm spatial resolution to ensure that resampling of the orthophoto mosaic resulted in a 15-cm ground sampling distance (GSD). Images were captured with 80% forward overlap and 30% lateral overlap to increase the number of instances per each subject point during the PPC generation process.

To characterize bare earth, we created a bare earth DTM using provincial LiDAR data collected from 2005 to 2008 and processed by the Government of Alberta (see Nagy-Reis et al., 2021; Van Rensen et al., 2015 for previous applications of these data). The LiDAR data were collected by Airborne Imaging with an average point density of 1.65 points/m², a vertical accuracy (maximum root-mean-square errors) of 0.30 m and horizontal accuracy of 0.45 m.

2.1.3 | Data processing

We processed the imagery to generate high-resolution multiband orthophoto mosaics and 3-dimensional (3D) point clouds. The imagery was organized into four blocks (Chinchaga 1, Chinchaga 2, Chinchaga 3 and Caribou Mountains) using the direct georeferencing information. We adjusted each block using an aerial triangulation bundle adjustment process to identify the position of photo centres and orientation of the camera at the moment of exposure. We used the GPS location of the centre of each photo, and exterior orientation angles to connect image coordinates to real-world locations. We determined the accuracy of each block adjustment by comparing randomly distributed elevation points to the bare earth DTM (Supplemental Information). The spatial accuracy of the aerial adjustments was within the expected specifications of three times the GSD of 15 cm.

Aerial imagery is distorted by the tilt of the camera, camera distortions and elevation changes in terrain. We therefore used

orthorectification to create a constant scale across aerial photos. We used the LiDAR-derived bare earth DTM as a base for orthorectification. The orthorectification process generated one ortho-photo per image with a spatial resolution of 15 cm GSD. We set the radiometric resolution to four spectral bands—Red, Green, Blue and Near-Infrared. Consequently, we used high-end colour balancing processing to produce a seamless mosaic over the entire project area. This process was semi-automatic, with manual quality control of generated seamlines, which were edited as needed. Finally, we generated 3D PPC from imagery using the Semi-Global Matching method and set the density of the point cloud to be one-pixel (GSD of 15 cm), resulting in an ultra-dense point cloud suitable for consequent detailed vegetation analysis. We used PHOTOMOD Version 7.2 for orthorectification and to generate point clouds.

We modelled tree-top locations in which to extract height to by analysing the PPC files with the R package `lidR` (Roussel et al., 2020). First, we normalized points to be relative to the ground surface using the wide-area LiDAR-derived bare earth DTM. We then modelled tree-top locations using the PPC by determining a location and height of each point cloud cluster using a local maximum filter (LMF). We used a variable window size for the LMF, depending on the height of the vegetation being measured. The window size was locked at 0.75 m for all points below 3 m, and at 3 m for all points higher than 17 m. Window size for vegetation between 3 and 17 m was computed by exponential function:

$$W = 3.5 * (-(\exp(-0.075 * (x - 1.55)) - 0.85)) + 1$$

We improved the algorithm through trial and error by projecting the 'LidR' output into the 3D softcopy stereomodels from optical imagery using DATEM Summit Evolution, and modifying the algorithm until vegetation tops matched the visible tops of vegetation in the softcopy stereomodels.

2.1.4 | Data analysis

For all feature types, the Alberta Biodiversity Monitoring Institute's Human Footprint Inventory (Alberta Biodiversity Monitoring Institute, 2018b) was used to delineate disturbance outlines. For polygonal disturbance types such as wellpads, pipelines and harvest areas, we combined the PPC-derived tree-top locations and assigned a height to each individual tree or shrub above 1 m tall by subtracting the LiDAR-derived DTM from the PPC-derived DSM. Features below 1 m may include non-canopy vegetation (such as grasses) and other features such as dirt piles, and thus were excluded. We then calculated vegetation density as the number of trees or shrubs above 1 m per unit area (hereafter termed 'tree density', though we do not discriminate between shrubs and trees) and the median height of trees for each disturbance polygon. We calculated median rather than mean height because polygon boundaries occasionally included trees adjacent to the human footprint, which disproportionately affects the mean.

Narrower linear features such as seismic lines and trails are often overshadowed by adjacent trees, and vegetation underneath the

adjacent canopy cannot be reliably classified using an automated process with PPC data (Dietmaier et al., 2019). We therefore used a manual classification process for these features. We modified centrelines for the seismic line corridors by manual stereomodel digitization at a scale of approximately 1:3000 to improve the spatial accuracy of interpreted seismic lines, which are less accurate than larger polygonal disturbances. For each seismic line segment connecting intersections with other features, we manually estimated vegetation type, density of each vegetation type (here assessed as percent cover from a bird's eye view) and average height of each vegetation type using stereo imagery interpretation (Supplemental Information). Vegetation was classified as coniferous trees, deciduous trees, shrubs, graminoids, lichens, bryophytes, non-vegetated and water following the Alberta Vegetation Inventory standards (Agriculture Forestry and Rural Economic Development, 2022), and reviewed against field photos during interpretation for quality assurance. We recorded the percent cover of the three most dominant vegetation types that were visible, and classified each segment of seismic line as the vegetation type with the highest percent cover value.

2.2 | Testing accuracy of vegetation height estimates

We used two approaches to test the accuracy of estimated vegetation heights from PPC-LiDAR fusion. First, we compared heights derived from PPC-LiDAR fusion to estimates from two other established techniques used within the study area: manual stereo image visualization, a long-established traditional technique for vegetation inventories and field measurements, which is considered the 'gold standard' data collection for validation (though see Luoma et al., 2017). Second, to validate the method's generalizability and to reduce the risk of overfitting to specific conditions or data set, in an independent study area we compared heights measured using manual stereo image visualization, field measurements, PPC-LiDAR fusion, and a state-of-the-art high-resolution multi-channel TiTAN LiDAR (see below).

Within our main study area, we sampled 120 sites distributed across the four areas where optical data were collected. Sites were selected to ensure sampling encompassed a range of disturbance types in a stratified random design (10 harvest area sites, 10 wellpads and 10 linear features sites). At each site, we took georeferenced photos to aid in interpretation of vegetation classes, and measured the height of three to five dominant or co-dominant canopy-layer trees spaced at least 10 m from each other. We stratified sampling equally across the most common tree species at each site. Trees under 2 m in height were measured using a reference pole with measurement markings, and those over 2 m in height were measured using a Vertex Hypsometer. We projected tree height measurements from field verification sites onto the 3D-stereomodels using the georeferenced photos to identify the exact tree that was measured in the field. We also projected the tree top locations generated by

the `lidR` package, with heights estimated by PPC-LiDAR fusion, onto the 3D-stereomodels. We visually estimated heights within the stereo environment using DATEM Summit Evolution.

To evaluate the strength of the relationship between measurements from the PPC-LiDAR fusion process to the field and stereo-model interpretation values, we first calculated Pearson correlation coefficients. We separated coniferous and deciduous trees and pooled observations across the four study area blocks. To further understand how PPC-LiDAR fusion estimates were related to these two other methods, and how this depended on tree type, we modelled the estimated tree height as a function of measurement method, interacting with tree type (deciduous vs. coniferous) as fixed effects and pooled observations across the study blocks.

Second, we used an independent data set in partnership with the Ecosystem Management Emulating Natural Disturbance (EMEND) Project (Figure 2). The EMEND research site is located in the Lower Foothills Ecoregion of Alberta, approximately 90km north-west of Peace River, and is within the Chinchaga caribou range (Figure 1). At the EMEND study site, multi-channel TiTAN airborne LiDAR system (Teledyne Optech, Ontario) was used to collect high-density point clouds. Multi-channel LiDAR was collected using a Piper Navajo survey aircraft on 8 August 2020. Survey parameters were 100kHz per channel with a 50-degree field of view, 32 Hz scan frequency and 50% swath sidelap. Ground speed was ~70m/s at an altitude of ~1000m above ground. Point density varied between 10 and 20points/m² and the relative elevation accuracy over selected tie planes was 0.04m.

TiTAN LiDAR point clouds were processed using the same workflow as above, but such that both vegetation structure and bare earth were estimated using the TiTAN LiDAR, using the package `lidR`. Field surveys were also conducted at 11 sites in the EMEND study area in August 2021 to measure three dominant or codominant trees at each site following the methods described above.

We acquired additional aerial imagery during the leaf-on season of 2020 (September 8). Using the same PPC-LiDAR workflow as above, we estimated individual tree heights using PPC derived from the aerial imagery and wide-area LiDAR. We also visually estimated heights within the stereo environment using DATEM Summit Evolution. We identified the same trees in each data set (TiTAN LiDAR, PPC-LiDAR fusion, stereomodels, and field data) by projecting the 'LidR' outputs and field-measured trees into the 3D softcopy stereomodels. We targeted dominant and codominant trees to improve our ability to measure the same trees using the different approaches, and as such we locked the window size for the LMF algorithm at 1m for all points below 2m, and at 3.5m for all points higher than 18m. We again optimized the algorithm through trial and error until vegetation tops match visible tops in the stereomodels. For vegetation between 2 and 18m, the window size was computed by the linear function:

$$W = x * 0.15 + 0.7.$$

We again evaluated the Pearson correlation between estimated heights from PPC-LiDAR fusion, TiTAN LiDAR, stereomodel visualization, and field measurements, then modelled the estimated tree

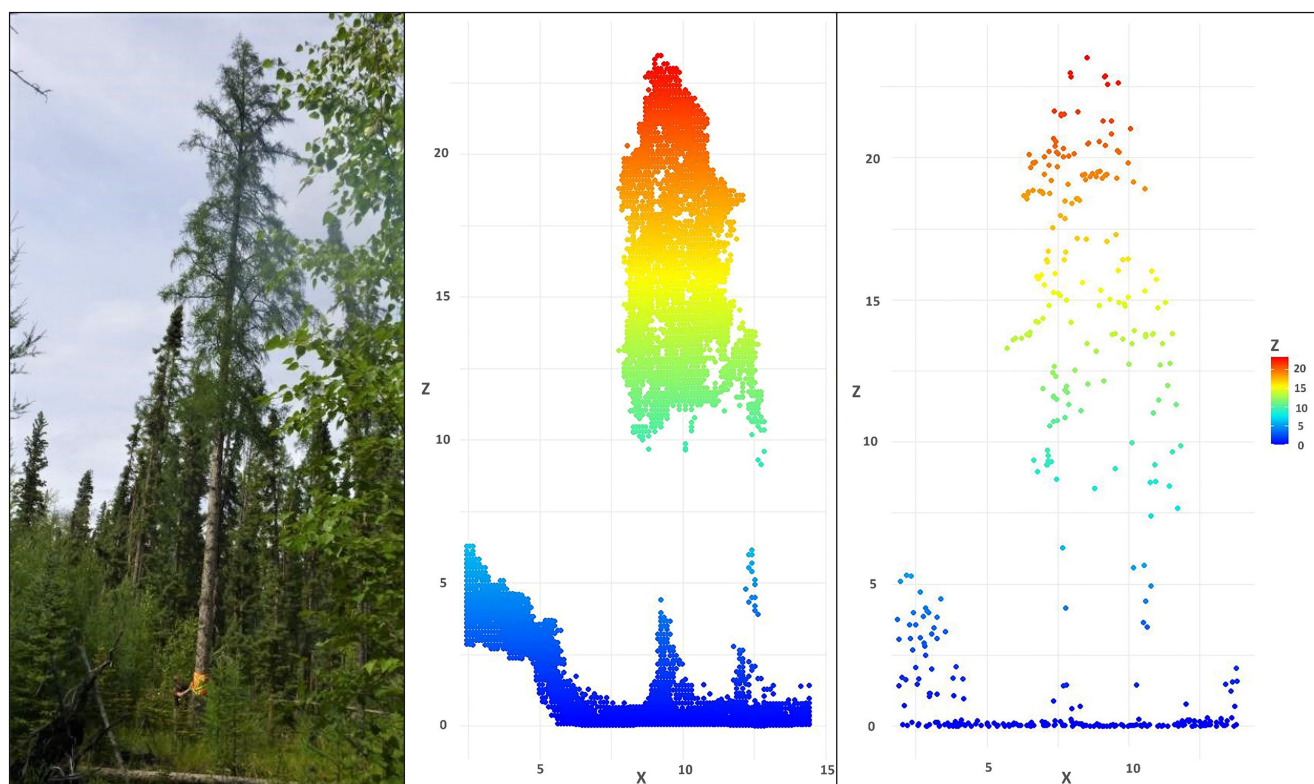


FIGURE 2 Example comparison of tree heights measured in the field (left), using PPC-LiDAR fusion (center) and TiTAN LiDAR (right). Z measurement indicates height in meters.

height as a function of measurement method, interacting with tree type (deciduous vs. coniferous) as fixed effects using a linear model (see [Supplemental Information](#) for more details).

3 | RESULTS

3.1 | Developing and applying PPC-LiDAR fusion

Vegetation on non-seismic polygonal disturbances in all study blocks had an average median height below 5 m ([Table 1](#)). There was considerable variation in average median heights across disturbances within study blocks as well as between study blocks ([Figure 3](#); [Supplemental Information](#)). All sites had some features with a median height above 10m, and some were as high as 24m. Harvest areas tended to have higher average median heights than wellpads and pipelines. Tree density on harvest areas and pipelines typically exceeded 1000/ha, whereas density on wellpads did not. The C1 site had the lowest mean median height on all feature types, and tended to have some of the lowest tree densities ([Table 1](#); [Figure 3](#)).

Most vegetation on seismic lines was under 1.5m, though there was variation between sites ([Figure 3](#); [Supplemental Information](#)). The CM site had the highest proportion of vegetation exceeding 5m and vegetation between 1.5 and 5m ([Table 2](#)). The remaining sites (C1, C2, and C3) had 2% or fewer seismic lines with vegetation exceeding 5m, and >65% under 1.5m. The majority of seismic lines were shrub dominated in CM and C3, but were dominated by a mix of shrubs and bryophytes in C1 and C2 ([Table 2](#); [Figure 3](#); [Supplemental Information](#)). Few seismic lines were dominated by either deciduous or coniferous trees, though CM had a total of 14% of seismic lines dominated by all tree species combined. Fewer than 1% of seismic lines were either dominated by lichens or were non-vegetated.

3.2 | Testing accuracy of vegetation height estimates

Within the main study area, tree heights estimated using PPC-LiDAR fusion were highly correlated with those estimated in the field ($r=0.87$ for coniferous; $r=0.93$ for deciduous; $p<0.05$) and using stereomodels ($r=0.98$ for coniferous; $r=0.97$ for deciduous; $p<0.05$). On average, trees heights estimated using PPC-LiDAR

fusion were 2.7m smaller than heights estimated in the field ($\beta=-2.723$, $SE=0.931$; $p<0.05$) but not different than using stereomodels ([Figure SI.1](#); [Table SI.2](#)).

In the independent study area, tree heights measured from PPC-LiDAR fusion, stereomodel interpretation, TiTAN LiDAR and field measurements were highly correlated ($r>0.97$, $p<0.05$, [Supplemental Information](#)). Tree heights derived from PPC-LiDAR fusion tended to be smaller than those measured from field measurements, stereomodel interpretation and TiTAN LiDAR, but there was no significant difference ($p<0.05$; [Figure 4](#); [Table SI.3](#)). Furthermore, the effect of measurement type did not differ between deciduous and coniferous trees ($p<0.05$; [Table SI.3](#)).

4 | DISCUSSION

Effective habitat management at local and landscape scales relies on accurate and consistent information about the vegetation community. We fused high-resolution PPC data with wide-area LiDAR data to collect high-resolution vegetation data consistently across human-altered habitat, and demonstrated operational applicability across large areas. We estimated the height and density of vegetation on polygonal features using a semi-automated process, as well as height and class (coniferous tree, deciduous tree, shrub, other) of vegetation on seismic lines through manual interpretation. We found that wellpads and pipelines were characterized by low density, short vegetation, whereas harvest areas were typically characterized by taller vegetation and a higher tree density. We also found limited vegetation on seismic lines, despite the fact that many of these human-created features were created decades ago (Pattison et al., 2016). Sparsely vegetated features were dominated by shrubs or low-lying vegetation such as bryophytes and graminoids, rather than coniferous or deciduous trees. Limited recovery of tree species on anthropogenic features, particularly seismic lines, is consistent with previous reports of stagnated regeneration on human-created features in the boreal forests of Alberta (Lee & Boutin, 2006; Nagy-Reis et al., 2021; Van Rensen et al., 2015).

Understanding vegetation recovery on human-altered habitat is particularly important when vegetation structure has been linked to the mechanisms of species' decline. Linear features such as pipelines and seismic lines facilitate increased predator movement, which is hypothesized to increase encounter rates with prey such as Threatened

TABLE 1 The mean of the median vegetation height (m) and density (trees/ha) on non-seismic human-altered habitat. Values are the median height of each feature, averaged by feature type. CM, Caribou Mountains; C1, Chinchaga 1; C2, Chinchaga 2; C3, Chinchaga 3.

Site	Average median height (m)				Density (trees/ha)			
	Pipelines	Wellpads	Harvest areas	Other features	Pipelines	Wellpads	Harvest areas	Other features
CM	3.6	2	—	2.9	1320	973	—	943
C1	2.6	1.9	—	2.1	1072	910	—	976
C2	3.7	3.4	4.3	3.4	1458	1245	1746	1249
C3	—	2.2	4.1	3	—	636	1933	2009

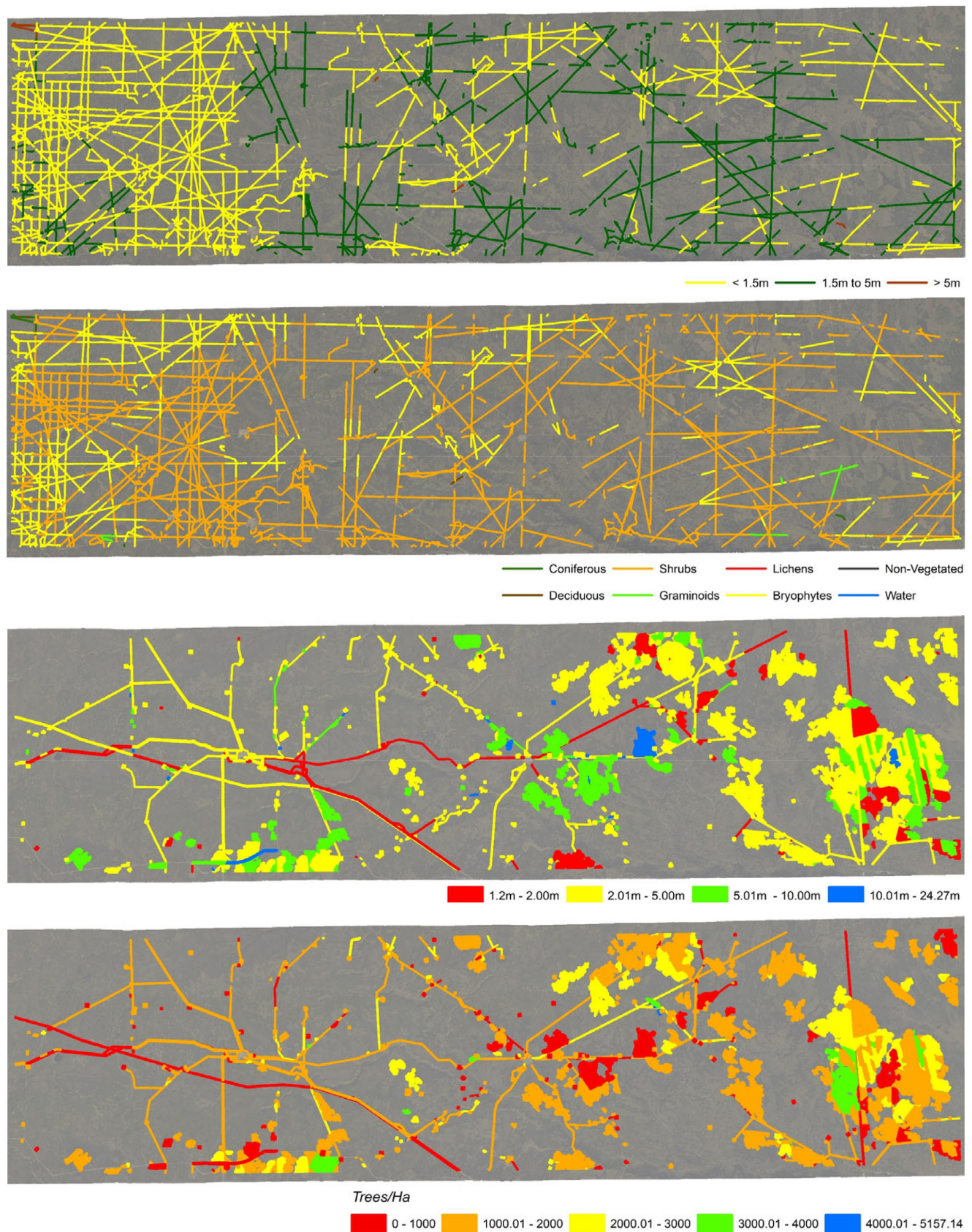


FIGURE 3 Example state of vegetation recovery on seismic lines and polygonal disturbances in the Chinchaga 3 block. From top to bottom, figures depict dominant vegetation type on 500-m sections of seismic line, the height of the dominant vegetation type on 500-m sections of seismic lines, median height (m) on non-seismic human footprint features and density (trees/ha) on non-seismic human footprint features.

TABLE 2 Percent area (%) of seismic lines covered by the dominant vegetation class, by height category and class. CM, Caribou Mountains; C1, Chinchaga 1; C2, Chinchaga 2; C3, Chinchaga 3.

Site	Percent area by vegetation height class			Percent area by vegetation class			
	>5 m	1.5–5 m	<1.5 m	Coniferous	Deciduous	Shrubs	Other
CM	11	46	42	5	9	72	15
C1	2	12	87	1	8	33	57
C2	1	21	78	0	0	49	51
C3	0	33	67	<1	<1	69	30

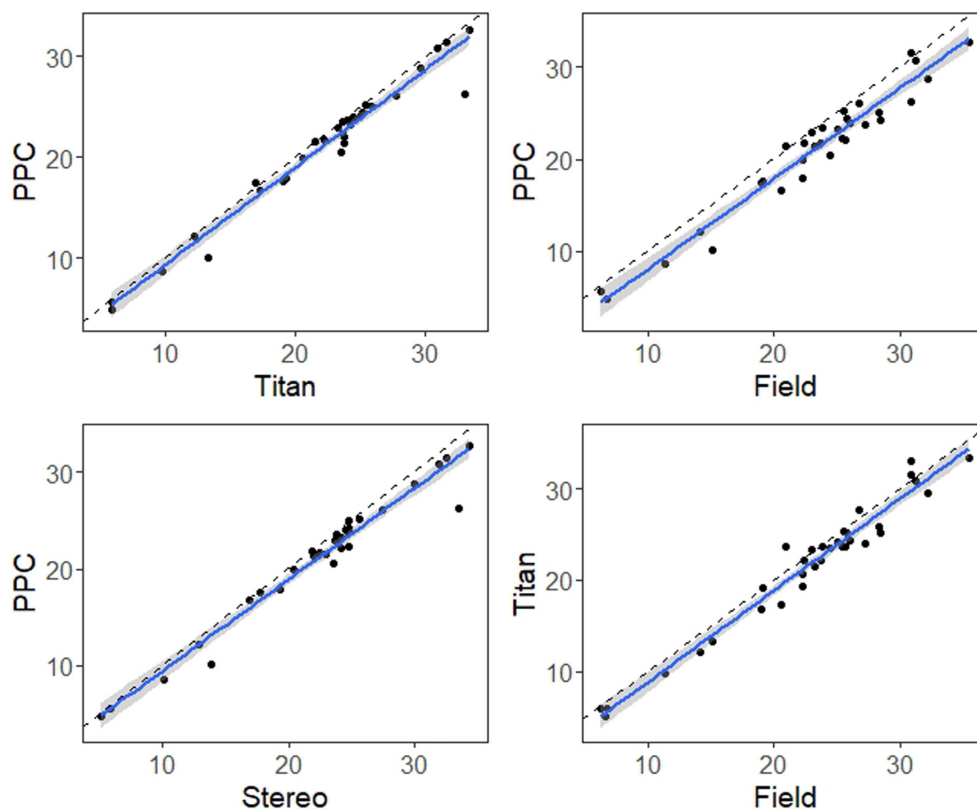


FIGURE 4 Vegetation heights (m) estimated using photogrammetry point cloud (PPC)-light detection and ranging (LiDAR) fusion, manual stereomodel visualization, TiTAN LiDAR, and field measurements. The blue line and shading represent a simple linear model for each plot and the associated 95% confidence intervals. The dashed line represents the 1 to 1 relationship. $N=33$ individual trees measured, though 2 were not measured using stereomodels and 1 was not measured using PPC because the individual tree could not be confidently identified.

caribou (Dickie, Serrouya, McNay, et al., 2017; McKenzie et al., 2012). Increased vegetation height, cover and roughness on linear features have been shown to slow the movement speed of wolves, presumably decreasing encounter rates with prey (Dickie, Serrouya, DeMars, et al., 2017; Finnegan, Pigeon, et al., 2018). In our study, few seismic lines exceeded vegetation heights previously found to reduce wolf travelling speed to that of surrounding forest (Dickie, Serrouya, DeMars, et al., 2017; Finnegan, Pigeon, et al., 2018). Indeed, the majority of seismic lines were characterized by vegetation heights below 1.5 m, suggesting that they may be near or below height thresholds found to slow wolf speeds even marginally (Dickie, Serrouya, DeMars, et al., 2017). In addition, vegetation rarely exceeded heights observed to deter human use of seismic lines (Pigeon et al., 2016). Continued human use of these features likely feeds back into limited

recovery as regenerating vegetation is continually disturbed (Van Rensen et al., 2015). Considering the composition of regenerating vegetation is also important, because increased shrub, graminoids and grass cover may increase forage availability for the apparent competitors of caribou (Finnegan, MacNearney, et al., 2018). Habitat restoration, with the goal of simultaneously returning forest cover and restoring predator–prey interactions, has been identified as a key management action for the recovery of boreal caribou populations (Environment and Climate Change Canada, 2020). It is estimated that habitat restoration will require billions of dollars given there are hundreds of thousands of kilometres of seismic lines alone (Johnson et al., 2019; Serrouya et al., 2020). Identifying where human-altered habitat is already recovering will help to prioritize habitat restoration activities into areas where vegetation regrowth is limited.

For many species at risk, detailed information on habitat status and trend is a limiting factor for effective habitat and species management. Fundamentally, informed decision-making requires an understanding of the mechanistic relationships that link habitat alteration to declines (North et al., 2017). From there, up-to-date information on habitat can be used to effectively plan and monitor management actions such as protection and restoration. Additionally, understanding the factors limiting regeneration can help target treatment types and intensity to increase restoration effectiveness (Suding, 2011). Previous investigations found that underlying habitat wetness was a predominant predictor of vegetation regeneration on seismic lines (Van Rensen et al., 2015). Van Rensen et al. (2015) used LiDAR-derived data with 2-m horizontal resolution to evaluate seismic line regeneration, which included well-balanced resolution and extent, given the technology that was available at that time. However, the LiDAR resolution was not sufficient to estimate metrics that reflect underlying mechanisms linked to wolf movements (Dickie, Serrouya, DeMars, et al., 2017). Linking wide-area mapping of post-disturbance recovery will further elucidate the driving factors of vegetation regeneration and allow more effective modelling of habitat structure across time and space.

To date, the gold standard for habitat inventories has been ground-based surveys. For example, field plots continue to be used to monitor post-disturbance and post-restoration recovery of caribou habitat (Government of Alberta, 2018). However, these surveys often present logistical and financial constraints, particularly in areas that are remote or otherwise difficult to access, have imperfect precision, and are impractical to extrapolate to broad scales (Luoma et al., 2017). Advances in remote sensing have accelerated the development of processes to monitor and inventory habitat at large scales (Bhatt et al., 2022; McDermid et al., 2005; Wulder et al., 2012). Even so, there is a trade-off between the scale of monitoring and the resolution of information acquired. To meet 'intermediate' needs, the combination of LiDAR, high-resolution imagery and satellite-based tools is promising (Queinnec et al., 2022; Wulder et al., 2007). We demonstrate the applicability of fusing high-resolution PPC and previously collected LiDAR to accurately measure vegetation across large areas, with the recognition that this is only one method available within the broader toolkit. Many previous applications of PPC and LiDAR to estimate forest structure and post-disturbance vegetation recovery have been promising, but limited to small areas (Gyawali et al., 2022; St-Onge et al., 2015; Ventura et al., 2022). Collecting LiDAR data at a fine enough resolution to estimate post-disturbance vegetation recovery is often cost-prohibitive at large scales. However, by pairing lower-resolution LiDAR, even with older vintages, with high-resolution and up-to-date optical data, which is less costly to collect and process than LiDAR, one can effectively estimate forest structure.

Our estimates provided sufficient accuracy to measure vegetation structure relevant to inform caribou habitat management using previously identified mechanisms of wolf movement, and to inform habitat status against government standards (Government of Alberta, 2018). Vegetation heights estimated using PPC-LiDAR

fusion were consistent with those estimated using traditional manual stereo image visualization and state-of-the-art TiTAN LiDAR, though field measurements underestimated heights relative to these other methods (see Luoma et al., 2017). This suggests that PPC-LiDAR fusion represents a promising tool to pair widely available, but coarse, LiDAR with high-resolution aerial imagery to inventory vegetation structure using a semi-automated process that is more efficient than traditional interpretation techniques, but lower cost than state-of-the-art LiDAR data. Continued technological improvements, such as machine learning, will improve processing power, automation and computing capacity (Bhatt et al., 2022; Gandomi & Haider, 2015). For example, automated fusion of LiDAR and PPC using machine learning will improve efficiencies and applicability across even larger scales still. The predominant limitation of our current approach is the inability to analyse understorey plants when the view is obstructed by tree canopies. Further integration of multispectral, hyperspectral, and LiDAR data using complex machine learning methods such as deep learning should improve the ability to estimate understorey vegetation structure by extracting complex patterns and relationships between vegetation characteristics and environmental factors. Fusion with additional free or low-cost satellite-based data will also expand the spatial and temporal scales in which vegetation structure can be monitored (Wulder et al., 2007), depending on the resolution of information needed to tie vegetation structure to the ecological mechanisms of interest. In addition to costs associated with collecting and processing high-resolution imagery, highly skilled analysts that are familiar with the analytical methods and study system is another barrier to upscaling our PPC-LiDAR approach, particularly for narrow linear features where manual interpretation is necessary.

Opportunities for the application of PPC-LiDAR fusion beyond the caribou habitat management context we provide are extensive, particularly where satellite-based data do not provide the resolutions required to match the ecological mechanisms in question, yet acquisition of high-resolution aerial- or terrestrial-based LiDAR is cost-prohibitive. Accurately measuring vegetation regenerating on forest harvest areas can contribute to sustainable forest management through informed harvest planning, assessment of growing stock, and optimized land-use planning (Wulder et al., 2008). Likewise, measuring forest regeneration following natural disturbances, such as wildfires and pest outbreaks, will be essential for forest management, particularly in the context of climate change (Brecka et al., 2020; Stralberg et al., 2018). Repeat measures of vegetation can be used for change detection (Tompalski et al., 2021), and to evaluate habitat restoration, as has been demonstrated in aquatic environments (Ventura et al., 2022). If the date of disturbance is known, or vegetation structure has been estimated at multiple time periods, vegetation recovery rates can be estimated using multivariate time series across the vast array of ecological conditions that this broad sampling will encompass. Finally, integrating high-resolution wide-area mapping with satellite-based time-series data provides the opportunity to evaluate trends in forest structure and composition over longer spatiotemporal scales (White et al., 2022; Wulder et al., 2007).

AUTHOR CONTRIBUTIONS

Melanie Dickie led the writing of this manuscript and contributed to data analysis. Branislav Hricko conceived the study design and methodology, and contributed to data analysis. Victor Tran contributed to data analysis. Christopher Hopkinson contributed to data analysis, manuscript preparation and provided TiTAN LiDAR data. Monica Kohler, Robert Serrouya and Sydney Toni contributed to manuscript preparation. Jahan Kariyeva supervised the study design and analysis.

ACKNOWLEDGEMENTS

We thank the Northwest Species at Risk Committee for funding portions of this work, as well as Phil Comeau for funding TiTAN data collection. We also thank Dr. Jonas Hagge and two anonymous reviewers for their valuable input on a previous version of this work.

CONFLICT OF INTEREST STATEMENT

The authors declare no conflict of interest.

PEER REVIEW

The peer review history for this article is available at <https://www.webofscience.com/api/gateway/wos/peer-review/10.1002/2688-8319.12254>.

DATA AVAILABILITY STATEMENT

Data are available from the Dryad Digital Repository <https://doi.org/10.5061/dryad.gxd2547rj> (Dickie et al., 2023).

ORCID

Melanie Dickie  <https://orcid.org/0000-0003-2177-2352>

Robert Serrouya  <https://orcid.org/0000-0001-5233-6081>

REFERENCES

- Agriculture Forestry and Rural Economic Development. (2022). *Alberta vegetation inventory standards manual*. Version 2.1.5.
- Alberta Biodiversity Monitoring Institute. (2018a). *The status of human footprint in Alberta*.
- Alberta Biodiversity Monitoring Institute. (2018b). *Wall-to-wall human footprint inventory*.
- Betts, M. G., Yang, Z., Hadley, A., Northrup, J., Nocera, J., Gorlick, N., Rousseau, J., Smith, A., & Gerber, B. (2022). Forest degradation drives widespread avian habitat and population declines. *Nature Ecology and Evolution*, 6(6), 709–719. <https://doi.org/10.1038/s41559-022-01737-8>
- Bhatt, P., Maclean, A., Dickinson, Y., & Kumar, C. (2022). Fine-scale mapping of natural ecological communities using machine learning approaches. *Remote Sensing*, 14, 1–25. <https://doi.org/10.3390/rs14030563>
- Brecka, A. F. J., Boulanger, Y., Searle, E. B., Taylor, A. R., Price, D. T., Zhu, Y., Shahi, C., & Chen, H. Y. H. (2020). Sustainability of Canada's forestry sector may be compromised by impending climate change. *Forest Ecology and Management*, 474, 118352. <https://doi.org/10.1016/j.foreco.2020.118352>
- Cavender-Bares, J., Schneider, F. D., Santos, M. J., Armstrong, A., Carnaval, A., Dahlin, K. M., Fatoyinbo, L., Hurtt, G. C., Schimel, D., Townsend, P. A., Ustin, S. L., Wang, Z., & Wilson, A. M. (2022). Integrating remote sensing with ecology and evolution to advance biodiversity conservation. *Nature Ecology and Evolution*, 6, 506–519. <https://doi.org/10.1038/s41559-022-01702-5>
- Coristine, L. E., Colla, S., Bennett, N., Carlsson, A. M., Davy, C., Davies, K. T. A., Favaro, B., Flockhart, D. T. T., Fraser, K., Orihel, D., Otto, S. P., Palen, W., Polfus, J. L., Venter, O., & Ford, A. T. (2019). National contributions to global ecosystem values. *Conservation Biology*, 33, 1219–1223. <https://doi.org/10.1111/cobi.13284>
- DeMars, C. A., & Boutin, S. (2017). Nowhere to hide: Effects of linear features on predator-prey dynamics in a large mammal system. *The Journal of Animal Ecology*, 87, 274–284. <https://doi.org/10.1111/1365-2656.12760>
- Díaz, S., Zafra-Calvo, N., Purvis, A., Verburg, P. H., Obura, D., Leadley, P., Chaplin-Kramer, R., De Meester, L., Dulloo, E., Martín-López, B., Shaw, M. R., Visconti, P., Broadgate, W., Bruford, M. W., Burgess, N. D., Cavender-Bares, J., DeClerck, F., Fernández-Palacios, J. M., Garibaldi, L. A., ... Zanne, A. E. (2020). Set ambitious goals for biodiversity and sustainability. *Science*, 370, 411–413. <https://doi.org/10.1126/science.abe1530>
- Dickie, M., Hricko, B., Hopkinson, C., Tran, V., Kohler, M., Toni, S., Serrouya, R., & Kariyeva, J. (2023). Data from: Applying remote sensing for large-landscape problems: Inventorying and tracking habitat recovery for a broadly distributed Species At Risk. *Dryad Digital Repository*. <https://doi.org/10.5061/dryad.gxd2547rj>
- Dickie, M., Serrouya, R., DeMars, C., Cranston, J., & Boutin, S. (2017). Evaluating functional recovery of habitat for threatened woodland caribou. *Ecosphere*, 8, 1–15. <https://doi.org/10.1002/ecs2.1936>
- Dickie, M., Serrouya, R., McNay, R. S., & Boutin, S. (2017). Faster and farther: Wolf movement on linear features and implications for hunting behaviour. *Journal of Applied Ecology*, 53, 253–263. <https://doi.org/10.1111/1365-2664.12732>
- Dietmaier, A., McDermid, G. J., Rahman, M. M., Linke, J., & Ludwig, R. (2019). Comparison of LiDAR and digital aerial photogrammetry for characterizing canopy openings in the boreal forest of northern Alberta. *Remote Sensing*, 11, 1–22. <https://doi.org/10.3390/rs1161919>
- Environment and Climate Change Canada. (2017). *Report on the progress of recovery strategy implementation for the woodland Caribou (Rangifer tarandus caribou), boreal population, in Canada for the period 2012–2017, species at risk act recovery strategy Series*.
- Environment and Climate Change Canada. (2020). *Agreement for the conservation and recovery of the woodland Caribou in Alberta*.
- Environment Canada. (2012). *Recovery strategy for woodland Caribou (Rangifer tarandus caribou), boreal population, in Canada*.
- Filicetti, A. T., Cody, M., & Nielsen, S. E. (2019). Caribou conservation: Restoring trees on seismic lines in Alberta, Canada. *Forests*, 10, 1–18. <https://doi.org/10.3390/f10020185>
- Finnegan, L., MacNearney, D., & Pigeon, K. E. (2018). Divergent patterns of understory forage growth after seismic line exploration: Implications for caribou habitat restoration. *Forest Ecology and Management*, 409, 634–652. <https://doi.org/10.1016/j.foreco.2017.12.010>
- Finnegan, L., Pigeon, K. E., Cranston, J., Hebblewhite, M., Musiani, M., Neufeld, L., Schmiegelow, F., Duval, J., & Stenhouse, B. (2018). Natural regeneration on seismic lines influences movement behaviour of wolves and grizzly bears. *PLoS ONE*, 13, e0195480.
- Foley, J., DeFries, R., Asner, G. P., Barford, C., Bonan, G., Carpenter, S. R., Chapin, F. S., Coe, M. T., Daily, G. C., Gibbs, H. K., Helkowski, J. H., Holloway, T., Howard, E. A., Kucharik, C. J., Monfreda, C., Patz, J. A., Prentice, I. C., Ramankutty, N., & Snyder, P. K. (2005). Global consequences of land use. *Science*, 309, 570–574.
- Fromm, M., Schubert, M., Castilla, G., Linke, J., & McDermid, G. (2019). Automated detection of conifer seedlings in drone imagery using convolutional neural networks. *Remote Sensing*, 11, 2585. <https://doi.org/10.3390/rs11212585>
- Gandomi, A., & Haider, M. (2015). Beyond the hype: Big data concepts, methods, and analytics. *International Journal of Information*

- Management, 35(2), 137–144. <https://doi.org/10.1016/j.jinforngt.2014.10.007>
- Government of Alberta. (2018). *Draft provincial restoration and establishment framework for legacy seismic lines in Alberta*. Government of Alberta 93.
- Gyawali, A., Aalto, M., Peuhkurinen, J., Villikka, M., & Ranta, T. (2022). Comparison of individual tree height estimated from LiDAR and digital aerial photogrammetry in young forests. *Sustainability*, 14, 3720. <https://doi.org/10.3390/su14073720>
- Hansen, M. C., Potapov, P. V., Moore, R., Hancher, M., Turubanova, S. A., Tyukavina, A., Thau, D., Stehman, S. V., Goetz, S. J., Loveland, T. R., Kommareddy, A., Egorov, A., Chini, L., Justice, C. O., & Townshend, J. R. G. (2013). High-resolution global maps of 21st-century forest change cover. *Science*, 342, 850–854. <https://doi.org/10.1126/science.1244693>
- Hebblewhite, M. (2017). Billion dollar boreal woodland caribou and the biodiversity impacts of the global oil and gas industry. *Biological Conservation*, 206, 102–111.
- Hopkinson, C., Chasmer, L., Gynan, C., Mahoney, C., & Sitar, M. (2016). Multisensor and multispectral LiDAR characterization and classification of a forest environment. *Canadian Journal of Remote Sensing*, 42, 501–520. <https://doi.org/10.1080/07038992.2016.1196584>
- Johnson, C. J., Mumma, M. A., & St-Laurent, M. (2019). Modeling multispecies predator–prey dynamics: Predicting the outcomes of conservation actions for woodland caribou. *Ecosphere*, 10, 1–28. <https://doi.org/10.1002/ecs2.2622>
- Jurado, J. M., López, A., Pádua, L., & Sousa, J. J. (2022). Remote sensing image fusion on 3D scenarios: A review of applications for agriculture and forestry. *International Journal of Applied Earth Observation and Geoinformation*, 112, 102856. <https://doi.org/10.1016/j.jag.2022.102856>
- Lee, P., & Boutin, S. (2006). Persistence and developmental transition of wide seismic lines in the western Boreal Plains of Canada. *Journal of Environmental Management*, 78, 240–250. <https://doi.org/10.1016/j.jenvman.2005.03.016>
- Luoma, V., Saarinen, N., Wulder, M. A., White, J. C., Vastaranta, M., Holopainen, M., & Hyypä, J. (2017). Assessing precision in conventional field measurements of individual tree attributes. *Forests*, 8, 38. <https://doi.org/10.3390/f8020038>
- McDermid, G. J., Franklin, S. E., & LeDrew, E. F. (2005). Remote sensing for large-area habitat mapping. *Progress in Physical Geography*, 29, 449–474. <https://doi.org/10.1191/0309133305pp455ra>
- McKay, T. L., Pigeon, K. E., Larsen, T. A., & Finnegan, L. A. (2021). Close encounters of the fatal kind: Landscape features associated with central mountain caribou mortalities. *Ecology and Evolution*, 11, 2234–2248. <https://doi.org/10.1002/ece3.7190>
- McKenzie, H., Merrill, E., Spiteri, R., & Lewis, M. (2012). How linear features alter predator movement and the functional response. *Interface Focus*, 2, 205–216.
- Mumma, M. A., Gillingham, M. P., Marshall, S., Procter, C., Bevington, A. R., & Scheideman, M. (2020). Regional moose (*Alces alces*) responses to forestry cutblocks are driven by landscape-scale patterns of vegetation composition and regrowth. *Forest Ecology and Management*, 481, 118763. <https://doi.org/10.1016/j.foreco.2020.118763>
- Nagy-Reis, M., Hebblewhite, M., Dickie, M., Calvert, A. M., Hervieux, D., Seip, D., Gilbert, S. L., Venter, O., DeMars, C., Boutin, S., & Serrouya, R. (2021). Habitat loss accelerates for the endangered woodland caribou in western Canada. *Conservation Science and Practice*, 3(7), e437. <https://doi.org/10.1111/csp2.437>
- Nasiri, V., Darvishsefat, A. A., Arefi, H., Griess, V. C., Sadeghi, S. M. M., & Borz, S. A. (2022). Modeling forest canopy cover: A synergistic use of sentinel-2, aerial photogrammetry data, and machine learning. *Remote Sensing*, 14, 1453. <https://doi.org/10.3390/rs14061453>
- Newbold, T., Hudson, L. N., Hill, S. L. L., Contu, S., Lysenko, I., Senior, R. A., Börger, L., Bennett, D. J., Choimes, A., Collen, B., Day, J., De Palma, A., Diaz, S., Echeverria-Londoño, S., Edgar, M. J., Feldman, A., Garon, M., Harrison, M. L. K., Alhusseini, T., ... Purvis, A. (2015). Global effects of land use on local terrestrial biodiversity. *Nature*, 520, 45–50. <https://doi.org/10.1038/nature14324>
- North, M. P., Kane, J. T., Kane, V. R., Asner, G. P., Berigan, W., Churchill, D. J., Conway, S., Gutiérrez, R. J., Jeronimo, S., Keane, J., Koltunov, A., Mark, T., Moskal, M., Munton, T., Peery, Z., Ramirez, C., Sollmann, R., White, A. M., & Whitmore, S. (2017). Cover of tall trees best predicts California spotted owl habitat. *Forest Ecology and Management*, 405, 166–178. <https://doi.org/10.1016/j.foreco.2017.09.019>
- Pattison, C. A., Quinn, M. S., Dale, P., & Catterall, C. P. (2016). The landscape impact of linear seismic clearings for oil and gas development in boreal forest. *Northwest Science*, 90, 340–354. <https://doi.org/10.3955/046.090.0312>
- Pigeon, K. E., Anderson, M., MacNearney, D., Cranston, J., Stenhouse, G., & Finnegan, L. (2016). Toward the restoration of caribou habitat: Understanding factors associated with human motorized use of legacy seismic lines. *Environmental Management*, 58, 821–832. <https://doi.org/10.1007/s00267-016-0763-6>
- Queinnec, M., Coops, N. C., White, J. C., Griess, V. C., Schwartz, N. B., & McCartney, G. (2022). Mapping dominant boreal tree species groups by combining area-based and individual tree crown LiDAR metrics with Sentinel-2 data. *Canadian Journal of Remote Sensing*, 49, 1–19. <https://doi.org/10.1080/07038992.2022.2130742>
- Queinnec, M., Coops, N. C., White, J. C., McCartney, G., & Sinclair, I. (2021). Developing a forest inventory approach using airborne single photon LiDAR data: From ground plot selection to forest attribute prediction. *Forestry*, 95(3), 347–362. <https://doi.org/10.1093/forestry/cpab051>
- Roussel, J.-R., Auty, D., Coops, N. C., Tompalski, P., Goodbody, T. R. H., Meador, A. S., Bourdon, J.-F., de Boissieu, F., & Achim, A. (2020). lidar: An R package for analysis of airborne laser scanning (ALS) data. *Remote Sensing of Environment*, 251, 112061. <https://doi.org/10.1016/j.rse.2020.112061>
- Serrouya, R., Dickie, M., DeMars, C., Wittmann, M. J., & Boutin, S. (2020). Predicting the effects of restoring linear features on woodland caribou populations. *Ecological Modelling*, 416, 108891. <https://doi.org/10.1016/j.ecolmodel.2019.108891>
- Serrouya, R., Dickie, M., Lamb, C., Van Oort, H., Kelly, A. P., Demars, C., McLoughlin, P. D., Larter, N. C., Hervieux, D., Ford, A. T., & Boutin, S. (2021). Trophic consequences of terrestrial eutrophication for a threatened ungulate. *Proceedings of the Royal Society B: Biological Sciences*, 288, 20202811. <https://doi.org/10.1098/rspb.2020.2811>
- Serrouya, R., McLellan, B. N., Boutin, S., Seip, D. R., & Nielsen, S. E. (2011). Developing a population target for an overabundant ungulate for ecosystem restoration. *Journal of Applied Ecology*, 48, 935–942. <https://doi.org/10.1111/j.1365-2664.2011.01998.x>
- St-Onge, B., Audet, F. A., & Bégin, J. (2015). Characterizing the height structure and composition of a boreal forest using an individual tree crown approach applied to photogrammetric point clouds. *Forests*, 6, 3899–3922. <https://doi.org/10.3390/f6113899>
- Stralberg, D., Wang, X., Parisien, M.-A., Robinne, F.-N., Sólomos, P., Mahon, C. L., Nielsen, S. E., & Bayne, E. M. (2018). Wildfire-mediated vegetation change in boreal forests of Alberta, Canada. *Ecosphere*, 9, e02156. <https://doi.org/10.1002/ecs2.2156>
- Suding, K. N. (2011). Toward an era of restoration in ecology: Successes, failures, and opportunities ahead. *Annual Review of Ecology, Evolution, and Systematics*, 42, 465–487. <https://doi.org/10.1146/annurev-ecolsys-102710-145115>
- Tompalski, P., Coops, N. C., White, J. C., Goodbody, T. R. H., Hennigar, C. R., Wulder, M. A., Socha, J., & Woods, M. E. (2021). Estimating changes in forest attributes and enhancing growth projections: A review of existing approaches and future directions using airborne 3D point cloud data. *Current Forestry Reports*, 7, 1–24. <https://doi.org/10.1007/s40725-021-00135-w>
- Tscharntke, T., Tylianakis, J. M., Rand, T. A., Didham, R. K., Fahrig, L., Batáry, P., Bengtsson, J., Clough, Y., Crist, T. O., Dormann, C. F.,

- Ewers, R. M., Fründ, J., Holt, R. D., Holzschuh, A., Klein, A. M., Kleijn, D., Kremen, C., Landis, D. A., Laurance, W., ... Westphal, C. (2012). Landscape moderation of biodiversity patterns and processes—Eight hypotheses. *Biological Reviews*, 87, 661–685. <https://doi.org/10.1111/j.1469-185X.2011.00216.x>
- Van Rensen, C. K., Nielsen, S. E., White, B., Vinge, T., & Liefvers, V. J. (2015). Natural regeneration of forest vegetation on legacy seismic lines in boreal habitats in Alberta's oil sands region. *Biological Conservation*, 184, 127–135. <https://doi.org/10.1016/j.biocon.2015.01.020>
- Ventura, D., Mancini, G., Casoli, E., Pace, D. S., Lasinio, G. J., Belluscio, A., & Ardizzone, G. (2022). Seagrass restoration monitoring and shallow-water benthic habitat mapping through a photogrammetry-based protocol. *Journal of Environmental Management*, 304, 114262. <https://doi.org/10.1016/j.jenvman.2021.114262>
- Wang, Y., Lehtomäki, M., Liang, X., Pyörälä, J., Kukko, A., Jaakkola, A., Liu, J., Feng, Z., Chen, R., & Hyyppä, J. (2019). Is field-measured tree height as reliable as believed—A comparison study of tree height estimates from field measurement, airborne laser scanning and terrestrial laser scanning in a boreal forest. *ISPRS Journal of Photogrammetry and Remote Sensing*, 147, 132–145. <https://doi.org/10.1016/j.isprsjprs.2018.11.008>
- Watson, J. E. M., Shanahan, D. F., Di Marco, M., Allan, J., Laurance, W. F., Sanderson, E. W., Mackey, B., & Venter, O. (2016). Catastrophic declines in wilderness areas undermine global environment targets. *Current Biology*, 26, 2929–2934. <https://doi.org/10.1016/j.cub.2016.08.049>
- White, J. C., Hermosilla, T., Wulder, M. A., & Coops, N. C. (2022). Mapping, validating, and interpreting spatio-temporal trends in post-disturbance forest recovery. *Remote Sensing of Environment*, 271, 112904. <https://doi.org/10.1016/j.rse.2022.112904>
- Wittmer, H. U., McLellan, B. N., Serrouya, R., & Apps, C. D. (2007). Changes in landscape composition influence the decline of a threatened woodland caribou population. *The Journal of Animal Ecology*, 76, 568–579. <https://doi.org/10.1111/j.1365-2656.2007.01220.x>
- Wittmer, H. U., Sinclair, A. R. E., & McLellan, B. N. (2005). The role of predation in the decline and extirpation of woodland caribou. *Oecologia*, 144, 257–267. <https://doi.org/10.1007/s00442-005-0055-y>
- Wulder, M. A., Bater, C. W., Coops, N. C., Hilker, T., & White, J. C. (2008). The role of LiDAR in sustainable forest management. *The Forestry Chronicle*, 84, 807–826. <https://doi.org/10.5558/tfc84807-6>
- Wulder, M. A., Han, T., White, J. C., Sweda, T., & Tsuzuki, H. (2007). Integrating profiling LiDAR with Landsat data for regional boreal forest canopy attribute estimation and change characterization. *Remote Sensing of Environment*, 110, 123–137. <https://doi.org/10.1016/j.rse.2007.02.002>
- Wulder, M. A., White, J. C., Nelson, R. F., Næsset, E., Ørka, H. O., Coops, N. C., Hilker, T., Bater, C. W., & Gobakken, T. (2012). LiDAR sampling for large-area forest characterization: A review. *Remote Sensing of Environment*, 121, 196–209. <https://doi.org/10.1016/j.rse.2012.02.001>
- Zhang, J., & Lin, X. (2017). Advances in fusion of optical imagery and LiDAR point cloud applied to photogrammetry and remote sensing. *International Journal of Image and Data Fusion*, 8, 1–31. <https://doi.org/10.1080/19479832.2016.1160960>

SUPPORTING INFORMATION

Additional supporting information can be found online in the Supporting Information section at the end of this article.

Table SI.1. Control projection center residuals. Mean absolute, RMS, and maximum are presented for each site. The number of points (differences) was 488 for Chinchaga 1, 495 for Chinchaga 2, 433 for Chinchaga 3, and 997 for Caribou Mountains.

Table SI.2. Linear model results evaluating the effect of measurement method on estimated tree heights (m). Measurement method interacting with tree type (deciduous vs. coniferous, with coniferous as the reference category) was included as fixed effects for each model, and observations across the study blocks were pooled.

Table SI.3. Linear model results evaluating the effect of measurement method on estimated tree heights (m) in the EMEND study site. Measurement method is included as an interaction with tree type (deciduous vs. coniferous). PPC-LiDAR fusion and coniferous trees are set as the reference category.

Figure SI.1. Vegetation heights (m) measured using photogrammetry point cloud–LiDAR fusion (PPC), photogrammetry stereomodels (Stereo), and field measurements (Field). Solid lines represent the simple linear model for each plot, separated by coniferous and deciduous vegetation types, and the associated 95 % confidence intervals. Dashed line represents the 1 to 1 relationship.

Figure SI.2. Comparison of tree heights measured using stereomodel visualization (stereo), field measurements (Field), TiTAN multi-spectral light detection and ranging (LiDAR) and photogrammetry point cloud (PPC)-LiDAR fusion.

Figure SI.3. Pearson correlation matrix of vegetation heights (m) measured using photogrammetry point cloud LiDAR fusion (PPC), photogrammetry stereomodels, TiTAN LiDAR and field measurements. $N=30$ individual trees were measured using all four methods.

Figure SI.4. State of vegetation on seismic lines and polygonal disturbances in the Chinchaga 1 study area block. From left to right, figures depict dominant vegetation type on 500m sections of seismic line, height of dominant vegetation type on 500m sections of seismic lines, median height (m) on non-seismic human footprint features and density (trees/ha) on non-seismic human footprint features.

Figure SI.5. State of vegetation on seismic lines and polygonal disturbances in the Chinchaga 2 study area block. From left to right, figures depict dominant vegetation type on 500m sections of seismic line, height of dominant vegetation type on 500m sections of seismic lines, median height (m) on non-seismic human footprint features and density (trees/ha) on non-seismic human footprint features.

Figure SI.6. State of vegetation on seismic lines and polygonal disturbances in the Chinchaga 3 block. From top to bottom, figures depict dominant vegetation type on 500m sections of seismic line, height of dominant vegetation type on 500m sections of seismic lines, median height (m) on non-seismic human footprint features and density (trees/ha) on non-seismic human footprint features.

Figure SI.7. State of vegetation on seismic lines and polygonal disturbances in the Caribou Mountains block. From top to bottom, figures depict dominant vegetation class on 500m sections of seismic line, height of dominant vegetation class on 500m sections of seismic lines, median height (m) on non-seismic human footprint features and density (trees/ha) on non-seismic human footprint features.

How to cite this article: Dickie, M., Hricko, B., Hopkinson, C., Tran, V., Kohler, M., Toni, S., Serrouya, R., & Kariyeva, J. (2023). Applying remote sensing for large-landscape problems: Inventorying and tracking habitat recovery for a broadly distributed Species At Risk. *Ecological Solutions and Evidence*, 4, e12254. <https://doi.org/10.1002/2688-8319.12254>